The origins of storm Ciarán: from diabatic Rossby wave to a warm-seclusion cyclone with a sting jet

The origins of Storm *Ciarán*: From diabatic Rossby wave to warm-seclusion cyclone with a sting jet

Ambrogio Volonté[1,2] **and Jacopo Riboldi**[3]

[1] *Department of Meteorology, University of Reading, Reading, UK*
[2] *National Centre for Atmospheric Science, University of Reading, Reading, UK*
[3] *Institute for Atmospheric and Climate Science, ETH Zurich, Zurich, Switzerland*

Introduction

The impacts caused by Storm *Ciarán* over several European regions motivate a detailed investigation of its synoptic evolution. Such analysis is presented here and illustrates the notable nature of *Ciarán*, not only for its impacts but also for its dynamics and lifecycle as an extratropical cyclone, including the physical processes that drove its rapid propagation and intensification.

Storm *Ciarán* originated as a diabatic Rossby wave (DRW; Parker and Thorpe, 1995; Moore and Montgomery, 2005). This peculiar family of cyclones exhibits several special dynamical features differentiating them from usual extratropical and tropical cyclones. These features have been discussed by Boettcher and Wernli (2013), who characterise DRWs as

- low-level systems, with a cyclonic circulation mostly confined below 700hPa, existing close to a strong baroclinic zone with intense low-level wind shear;
- driven by latent heat release, which is particularly strong just downstream of the cyclone centre (where moist air encounters the baroclinic zone and ascends);
- propagating rapidly along the baroclinic zone, following a propagation mechanism independent from the jet stream and that involves a continuous re-generation of the storm in the region of latent heat release.

As DRWs approach regions of ascent embedded in the jet stream (e.g. the jet left-exit), they can encounter favourable conditions for intensification as 'normal' extratropical cyclones (Rivière *et al.*, 2010; Boettcher and Wernli, 2011). The presence of a pre-existing low-level vorticity maximum associated with the DRW, in a context of high baroclinicity and intense latent heat release, can make such an intensification very rapid or 'explosive', as it was the case for the extreme Storm *Lothar* (which also originated from a DRW, as shown by Wernli *et al.*, 2002) and for the Autumn 1991 'Perfect Storms' (Cordeira and Bosart, 2011).

Rapid intensification did indeed occur in the case of Storm *Ciarán* and resulted in the development of a warm seclusion, that is a warm cyclone core at low levels. The development of warm seclusions in extratropical cyclones is described in the Shapiro–Keyser conceptual model of cyclone evolution (Shapiro and Keyser, 1990). The classic Norwegian cyclone model, presented more than a century ago (see Bjerknes, 1919; Bjerknes and Solberg, 1922), is still regarded as a remarkable scientific achievement, serving as foundation for synoptic meteorology and for the analysis of the structure and evolution of extratropical cyclones. However, over the years it gradually became clear that there were inconsistencies between the Norwegian model and observed frontal structures, particularly in some cyclones. This led to refinements to the conceptual model and the developments of alternative models, such as the Shapiro–Keyser model (Dacre, 2020). The Shapiro–Keyser model is characterised by a weakening of the higher-latitude part of the cold front and the opening of a frontal fracture region, with the remaining part of the cold front nearly perpendicular to the warm front. As the cyclone evolves towards maturity, the warm front gradually encircles the cyclone centre, becoming a bent-back front and eventually wrapping around the centre. As it does so, it leads to the formation of a warm seclusion at the low-level cyclone core (Schultz and Vaughan, 2011).

Warm-seclusion cyclones are also associated with extreme windstorms and with the development of sting jets. A sting jet is an air stream that descends from mid-levels off the tip of the cloud head into the frontal fracture region of an extratropical cyclone. It is a short-lived and small-scale feature, but it can lead to extreme surface winds (Clark and Gray, 2018) and sting jets have been identified in several of the most damaging windstorms affecting northwest Europe in recent years. As explained in the previous paragraph, the opening of a frontal fracture region is a feature of the cyclones following the Shapiro–Keyser model, that is, those developing a warm seclusion.

In this work, we show that Storm *Ciarán* fulfilled the DRW criteria established in the climatological study by Boettcher and Wernli (2013) and we describe its evolution from DRW to a warm-seclusion cyclone that included extreme winds caused by sting jets. To our knowledge, this pathway has not yet been discussed explicitly in the literature and we argue its relevance to the understanding of extreme windstorms.

Ciarán as a diabatic Rossby wave

Storm *Ciarán* was first identified as a cyclone on the evening of 30 October 2023 off the east coast of the United States. In its first life stages, it appeared as a small, 990hPa-deep low-pressure system propagating along a zonally oriented baroclinic zone over the western North Atlantic (Figure 1a). The depression was located close to the right exit of a rather strong, zonally oriented jet stream and did not exhibit clear surface fronts; however, it featured heavy precipitation just to the east of the circulation centre. That area of precipitation corresponded to a region of strong low-level moisture flux convergence (MFC), particularly evident when convergence is computed in a frame of reference moving with the storm as in Figure 1b. At this stage, *Ciarán* was propagating eastward at a speed between 25 and 30ms^{-1} (Figure 1d); this very rapid motion resulted in very strong winds for a 990hPa-deep cyclone, with a 850hPa wind maximum just shy of 40ms^{-1} to the south of the storm centre, as shown later in Figure 3a.

These characteristics already point to the DRW nature of Storm *Ciarán*, that in these early stages indeed fulfilled the criteria used by Boettcher and Wernli (2013) to objectively define DRWs:

1. presence of a closed sea-level pressure minimum;

Ambrogio Volonté and Jacopo Riboldi contributed equally to this work.

RMetS Royal Meteorological Society

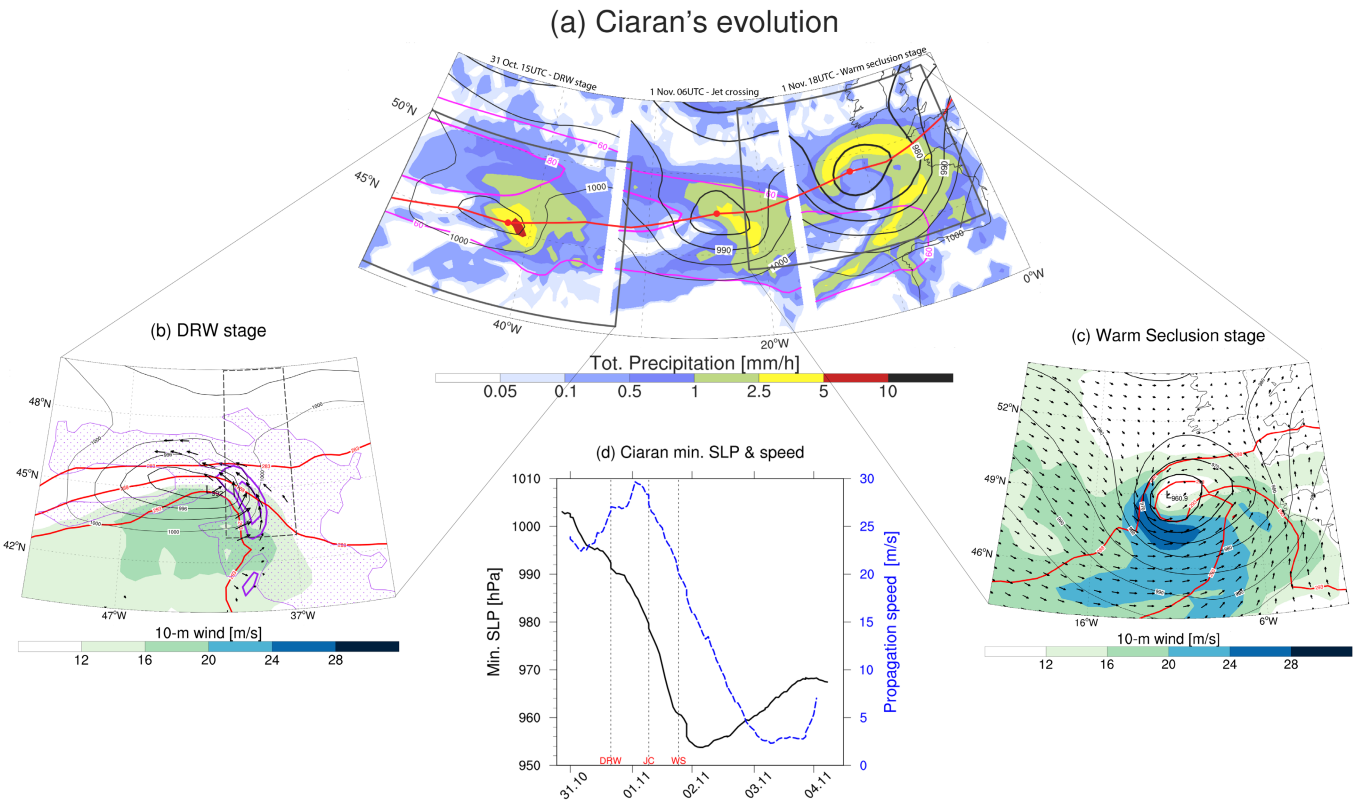

Figure 1. Evolution of Storm Ciarán *from diabatic Rossby wave to warm-seclusion cyclone, diagnosed from ERA5 Reanalysis data (Hersbach* et al., *2020). (a) Precipitation (in mmh^{-1}, shaded), sea-level pressure (black contours, in steps of 5hPa between 1000hPa and 980hPa, then in steps of 10hPa) and 250hPa wind (magenta contours, in steps of 15ms^{-1} between 60ms^{-1} and 90ms^{-1}) at three relevant time steps. Cyclone track and positions at such time steps are depicted by the red line and dots. (b) Zoom on the DRW stage (31 October 2023, 1500 UTC): 10m mean wind (shaded), sea-level pressure (black contours, in steps of 2hPa between 1000hPa and 990hPa), 950hPa potential temperature (red contours, only 283K, 288K and 293K) and, both storm-relative, 850hPa moisture flux convergence (purple contours, only 0.5 × 10^{-3} s^{-1} and 1 × 10^{-3} s^{-1}) and 850hPa moisture flux (black arrows, only in grid points with MFC > 0.25 × 10^{-3} s^{-1}). Purple stippling marks grid points where 850hPa relative humidity exceeds 95%. (c) Zoom on the warm seclusion stage (1 November 2023, 1800 UTC): 10m wind and equivalent potential temperature as in (b), wind direction indicated by black arrows. (d) Minimum sea-level pressure (black) and propagation speed (blue) of Storm* Ciarán *during its evolution.*

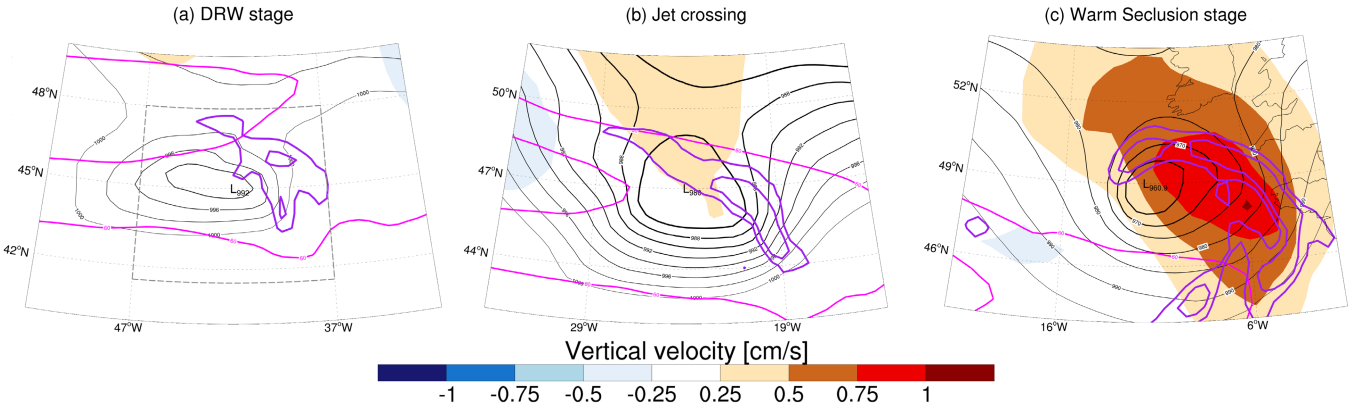

Figure 2. Vertical velocity patterns forced by upper layers (diagnosed from ERA5 Reanalysis data). Quasi-geostrophic vertical velocity at 700hPa due to vorticity and temperature advection in the upper layer (550–200hPa; in cms^{-1}, shaded) and full vertical velocity at 700hPa (purple contours, only 10, 20cms^{-1}) at the same relevant time steps plotted in Figure 1. Overlaid are sea-level pressure and 250hPa wind (black and magenta contours, respectively, contour values as in Figure 1). Dashed grey segments in (a) indicate the averaging domain used to evaluate whether the upper-level forcing for ascent fulfils the DRW criterion.

2. very weak forcing for ascent induced by the upper levels, with an upper cap of 0.5cms^{-1} to 700hPa vertical velocity averaged over the region of the cyclone (*Ciarán* featured values broadly below 0.25cms^{-1}, evaluated in the light grey box in Figure 2a; more details about the assessment of forcing for ascent are provided in "Vertical velocity decomposition" section).
3. presence of a low-level potential vorticity maximum exceeding 0.8 PVU at 850hPa (potential vorticity values at this level exceeded 2 PVU in *Ciarán*, see Figure 3a);
4. presence of substantial low-level baroclinicity at 950hPa in to the east of the low, with a $\Delta\theta_w$ between the warmest and the coldest temperature of at least 5K ($\Delta\theta$ exceeded 8K in *Ciarán*, see the dark grey box in Figure 1b);

5. fast propagation of the cyclone, exceeding at least 11.6ms^{-1} over a 6-h period (*Ciarán* featured a propagation speed more than twice as high as the threshold, see Figure 1d);
6. sufficiently high 850hPa relative humidity (RH) in the cyclone environment, with the 10% highest relative humidity values that have to exceed RH > 90% (*Ciarán* featured RH values well above 95% around the cyclone, see stippling in Figure 1b);

All the above listed criteria were fulfilled for a total of 21h (between 1800 UTC 30 November and 1500 UTC 31 November 2023), thus overcoming the 18-h threshold employed in the climatology of Boettcher and Wernli (2013): the analysis confirms that *Ciarán* was indeed a DRW in its initial stages. Afterwards, the storm crossed the jet stream in the morning of 1 November (Figure 1a, central panel) and started to explosively deepen (with a pressure drop of around 32hPa between 0000 UTC 1 November and 0000 UTC 2 November, well above the threshold for explosive cyclogenesis, see Sanders and Gyakum (1980)) and evolve into a warm-seclusion cyclone.

The rightmost panel of Figure 1a illustrates the outcome of this evolution, together with Figure 1c. After having crossed the jet stream, *Ciarán* evolved into a deep cyclone with precipitation organised in a comma-shaped pattern, following the main fronts (not shown). Strong low-level winds were present south of the cyclone centre, which was at that time characterised by a local maximum in low-level potential temperature, namely, a warm seclusion. The evolution of Storm *Ciarán* into an intense warm-seclusion cyclone is described in more detail in the "*Ciarán* evolves from diabatic Rossby wave to warm-seclusion cyclone containing a sting jet" section.

Vertical velocity decomposition

The assessment of the last DRW criterion involves a quantification the portion of vertical velocity forced by upper levels and deserves a more in-depth explanation. The contribution of the upper troposphere to vertical velocity can be diagnosed by inverting the omega equation (Box 1).

The decomposition described in Box 1 reveals some interesting dynamical features of Storm *Ciarán* (Figure 2). First, as already mentioned, *Ciarán* was located in its initial DRW stage at the right exit of a jet streak (Figure 1a), an area with little forcing for ascent provided by upper levels: this is depicted in Figure 2a by the very low values, close to zero, of vertical velocity forced by upper levels. The southward advection of warm air towards the sloped baroclinic zone to the right of the storm forces a minor degree of ascent (not shown). However, the actual vertical velocity is up to two orders of magnitude higher than that derived from the omega equation and is localised close to region of maximum precipitation (Figure 2a). Such high values are associated with the strong latent heat release in the region of heavy precipitation, a process which is not captured in the dry, quasi-geostrophic framework of the omega equation.

The contribution from upper levels started to increase as the storm crossed the jet stream from south to north and entered the left-exit region (Figure 2b) and continued to grow as *Ciarán* intensified explosively (Figure 2c). The overlap between the low pressure centre and the area of strong ascent driven by latent heat release likely contributed to the observed rapid intensification and to the associated strong surface winds, as expected from climatological studies (e.g. Binder *et al*., 2016; Stanković *et al*., 2024). However, as the storm reached a more mature stage, the strong precipitation-driven ascent moved away from the centre of the storm towards the frontal region, limiting its capability to influence central pressure (Figure 2c); this observation emphasises the role of the persistent, broad large-scale ascent driven by upper levels (and lower levels, not shown) in driving storm intensification, a substantial change with respect to the earlier DRW regime.

Ciarán evolves from diabatic Rossby wave to warm-seclusion cyclone containing a sting jet

Storm *Ciarán* evolved from a diabatic Rossby wave to a warm-seclusion cyclone. This is illustrated by the maps and vertical cross-sections contained in Figure 3, which refer to the same times chosen in Figure 1a to represent the three stages of its evolution, namely, the development as DRW followed by the northward crossing of the jet stream and the subsequent formation of a warm seclusion at the centre of the cyclone.

Figure 3a,b refer to 1500 UTC on 31 October, the same time as the leftmost panel in Figure 1a. These figures illustrate the DRW status of Storm *Ciarán* early in its evolution, highlighting the high values of potential vorticity at low levels at the frontal boundary between tropical and mid-latitude air masses. At this time the surface cyclone is still several hundreds of kilometres south of the core of the jet stream and of no regions of high upper-level potential vorticity are visible in the vertical section. Hence, as already highlighted in the "Vertical velocity decomposition" section, it lies in an area which would be unfavourable to the development of a low-level cyclone if it were to be primarily driven by interaction with the upper-level flow. As noted in "*Ciarán* as a diabatic Rossby wave" section, strong low-level winds are present to the south of the cyclone centre and of the region of low-level potential vorticity exceeding 2 PVU, with peak values almost reaching 40ms^{-1}. These wind speeds are normally associated with intense and fully developed windstorms, rather than shallow cyclones in the early stages of their lifecycle. However, in this case strong winds are favoured by the storm motion exceeding 25ms^{-1}, consistent with its DRW status; see the "*Ciarán* as a diabatic Rossby wave" section and Figure 1.

Figure 3c,d refer to 0600 UTC on 1 November, the same time as the central panel in Figure 1a. This is when the surface cyclone crosses the axis of the upper-level jet and is about to enter the most rapid phase of its deepening (see Figure 1d). The contours of

Box 1.

The omega equation is used to diagnose vertical motion in a quasi-geostrophic framework; see Hoskins *et al*. (1978) and Davies (2015). It can be applied to determine the patterns of lower-tropospheric ascent and descent providing as input only the wind and temperature values in the upper troposphere, defined in this study as the 550- to 200hPa layer. The resulting vertical velocity field extends outside that layer and reaches lower levels too; this is consistent with the known paradigm of interaction between the upper and the lower levels of the troposphere during cyclogenesis (e.g. Hoskins *et al*., 1985). The vertical velocity ω (in Pa s^{-1}) forced by the upper troposphere is diagnosed at the level of 700hPa to assess the DRW criterion, following Boettcher and Wernli (2013). The resulting vertical velocity values w are converted from Pa s^{-1} to cms^{-1} using the approximate relationship.

$$w = -\frac{\omega}{g\rho_{700}} = -\omega\frac{R_d T_{700}}{g p_{700}} \quad (1)$$

where p_{700} = 700hPa, ρ_{700} and T_{700} correspond to the density and the temperature at the same level, g = 9.806ms^{-2} is the acceleration due to gravity and $R_d = 287\frac{\text{J}}{\text{kg}\cdot\text{K}}$ is the ideal gas constant for dry air.

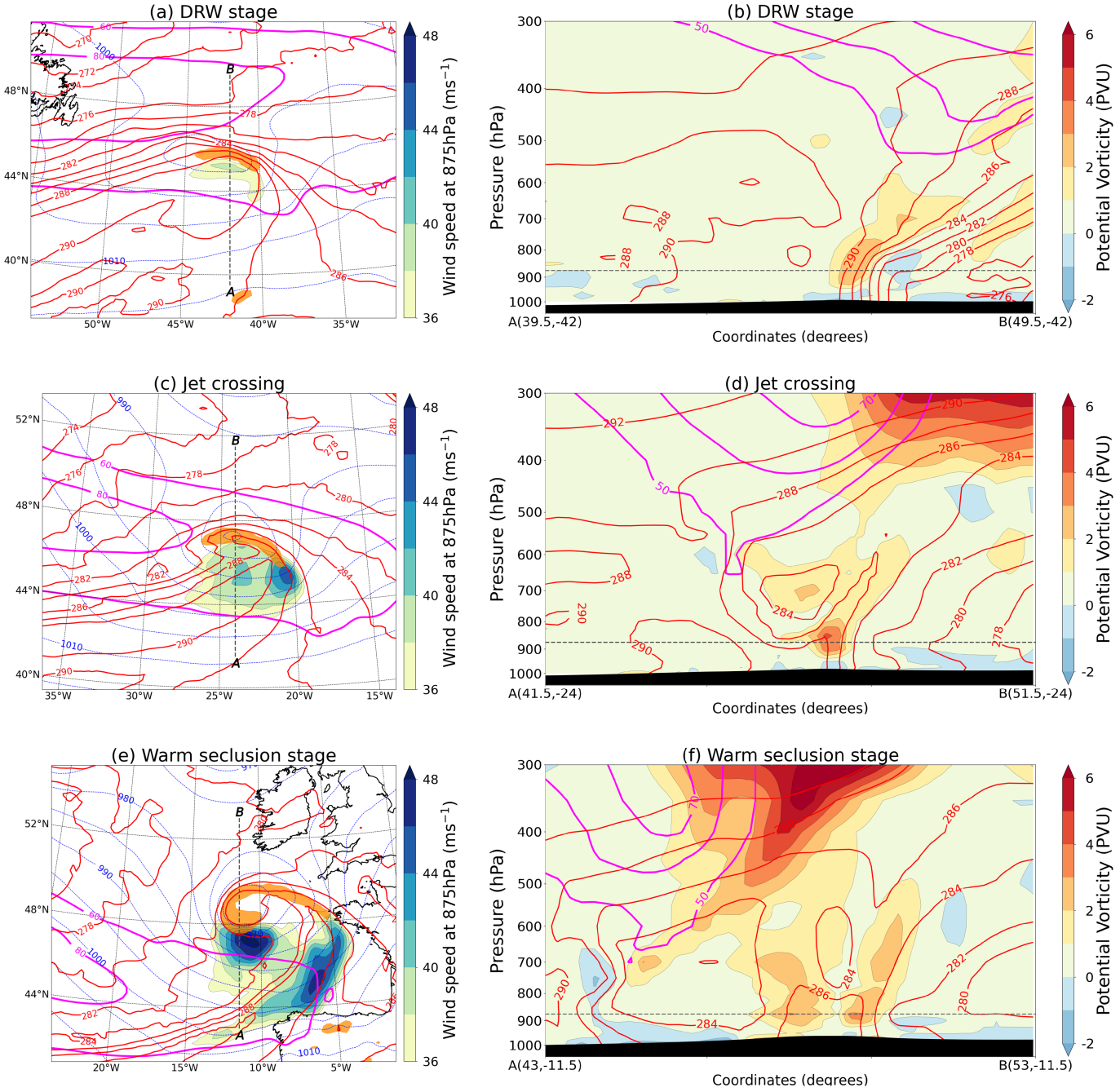

Figure 3. Maps and vertical cross-sections displaying the evolution of Storm Ciarán *across stages, using ERA5 Reanalysis data. Panels (a,c,e): maps of wind speed (yellow-to-blue shading), potential vorticity (values above 2 PVU, orange shading) and wet-bulb potential temperature (red contours every 1K), all at 875hPa. The maps also display wind speed at 250hPa (magenta contours from 60ms^{-1} every 20ms^{-1}) and mean sea-level pressure (thin blue dashed contours every 5hPa). Panels (b,d,f): vertical cross-sections on AB transects of potential vorticity (shading), wet-bulb potential temperature (red contours every 2K), wind speed (thick magenta contours from 50ms^{-1} every 10ms^{-1}). Grey dashed lines indicate in panels (a,c,e) the locations of the vertical section transects and in panels (b,d,f) the pressure level of the maps.*

wet-bulb potential temperature in the map illustrate the southeastward motion of the cold front, on the western side of the surface cyclone, while the warm front moves north. Strong low-level winds span the whole southern side of the cyclone, where the storm motion (still faster than 25ms^{-1}) adds up to the cyclonic circulation around the cyclone. Wind speed is especially high, exceeding 44ms^{-1}, in a small region of the warm sector to the southwest of the surface cyclone, where it indicates the presence of a developing warm conveyor belt. The vertical cross-section shows the upper-level jet now over the low-level potential vorticity maximum, with high values of potential vorticity on its polar side. A full *PV tower* (Čampa and Wernli, 2012) is thus forming, with a region of high potential vorticity also present at mid levels. This region, centred at around 700hPa, is associated with values of wet-bulb potential temperature lower than the surroundings. It indicates the arrival of the dry intrusion, an air stream identifiable by the wedge-shaped dry slot in satellite imagery and that descends from near the tropopause towards the lower troposphere as the cyclone deepens and its tropopause folds (Raveh-Rubin, 2017). In this case the dry intrusion is still clearly visible several hours later, as in Figure 4.

Figure 3e,f refer to 1800 UTC on 1 November, the same time as the rightmost panel in Figure 1a. At this time Storm *Ciarán* has completed its rapid deepening, occurring under the favourable left-exit region of the jet stream, and has developed into an intense warm-seclusion cyclone. A warm core is now visible at low levels, encircled by cooler air (see 286K wet-bulb potential temperature contour in both map and vertical section). Strong winds are present in the

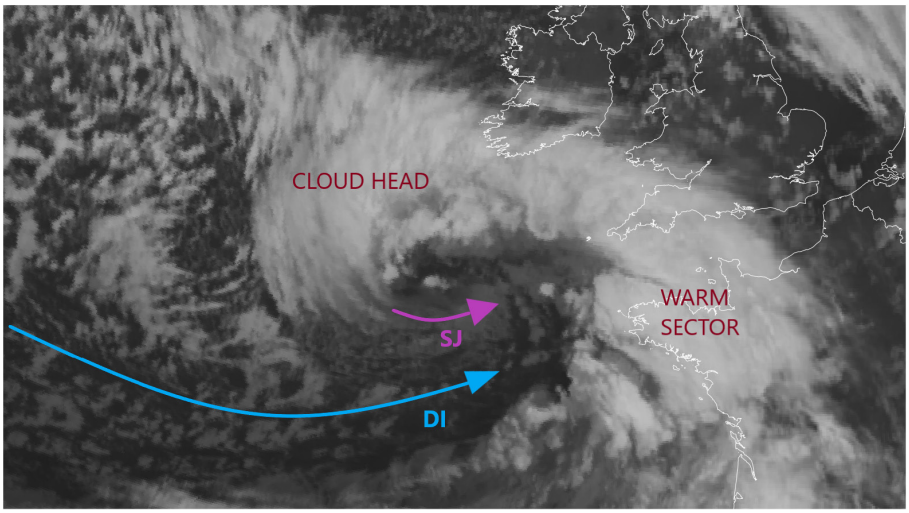

Figure 4. Infrared (10.8μm channel) High Rate SEVIRI image from the Meteosat second-generation 0° satellite referring to 1730 UTC on 1 November 2023 (©EUMETSAT [2023]), with added indications of the paths of sting jet and dry intrusion and the locations of cloud head and warm sector.

warm sector and to the south of the cyclone centre, respectively exceeding 46ms^{-1} and 48ms^{-1}. The former wind maximum indicates the warm conveyor belt, while the latter lies in the frontal fracture region, an area of weak thermal gradients located behind the primary cold front (indicated in Figure 4 by the western edge of the warm-sector cloud) and ahead of the cloud-head tip.

As explained in "*Ciarán* as a diabatic Rossby wave" section, the opening of a frontal fracture region is characteristic of Shapiro–Keyser cyclones and is where a sting jet would descend towards the top of the boundary layer. Sting jets cannot be fully resolved by ERA5 and therefore the frontal-fracture wind maximum in Figure 3e does not properly indicate one. It is rather the result of synoptic-scale cyclonic motion around the deep cyclone centre, the storm motion being still fast and in the same direction, and is possibly enhanced by the arrival of the cold conveyor belt and by low-level divergence at the end of the bent-back warm front (see Clark and Gray (2018) and Schultz and Sienkiewicz (2013)). It can thus be inferred that a sting jet descending in the region would lead to even higher wind speeds. This is consistent with the results in Gray and Volonté (2024) who, analysing operational forecasts of Storm *Ciarán* from the operational NWP model from the UK Met Office (with a grid spacing of roughly 10km in the region), highlight the descent of two distinct sting jets with maximum wind speeds exceeding 52ms^{-1} at 850hPa. Figure 4 also provides a clear indication of sting jet descent with extensive banding at the tip of the cloud head. These bands are caused by slantwise circulations and by the release of mesoscale instabilities associated with the descent of sting jets (Browning, 2004). Further evidence is provided by the onset of shallow convection ahead of the banding and near the cyclone centre, caused by the impact of the fast-moving and descending sting jet against slower-moving air at the top of the boundary layer (Browning and Field, 2004).

Discussion

The results presented throughout this article illustrate the evolution of Storm *Ciarán* from DRW to an intense warm-seclusion extratropical cyclone, capable of producing sting jets. DRWs are known precursors to explosively intensifying cyclones when the diabatically generated low-level potential vorticity favourably interacts with the upper-level circulation, but their specific evolution into warm-seclusion cyclones potentially bearing sting jets has not yet been explored.

As explained in the Introduction, cyclones developing a warm seclusion are characterised by a frontal fracture region in which sting jets can descend and accelerate, consistent with the Shapiro–Keyser conceptual model of cyclone evolution. There has been considerable research on which upper-level flow configurations are the most favourable for the development of Shapiro–Keyser cyclones. Schultz *et al*. (1998) used case studies and idealised simulations to highlight how a confluent background flow is more conducive to that evolution, while Norwegian cyclones are favoured by a diffluent background flow. Thorncroft *et al*. (1993) explored instead the effects of horizontal wind shear across the upper-level jet, through idealised simulations. They presented two different life cycle models, LC1 and LC2, that have proved extremely useful in many different real-world analyses (Catto, 2016), both developing a surface warm seclusion at different stages of their evolution. However, these works and the many others building on them are all considering surface anomalies that interacting with the upper-level flow directly above them from the beginning of the lifecycle, leading to the development of the cyclone. In the early phases of Storm *Ciarán's* evolution, that is, its DRW stage, the development is only driven by the interaction between the near-surface temperature gradients and the low-level diabatic processes. The upper-level jet core is still to the north of the surface cyclone and its influence on early cyclone development is negligible. Results in the "Vertical velocity decomposition" section illustrate how the upper-level forcing only starts contributing to cyclone intensification when the surface cyclone crosses the upper-level jet axis.

We thus focus on research investigating the evolution of surface cyclones that, as in the case of Storm *Ciarán*, initially developed south of the jet core, with diabatic processes playing a primary role in their evolution. Coronel *et al*. (2016) used idealised simulations to show that surface cyclones initialised on the warm side of the upper-level jet, rather than directly underneath it, are more likely to evolve according the Shapiro–Keyser model, develop a bent-back warm front and warm seclusion and, when horizontal and vertical resolutions are fine enough, display the formation and descent of a sting jet. Coronel *et al*. (2015) also pointed out the role of moist processes in enhancing the northward motion of mid-latitude surface cyclones, helping them to cross the upper-level jet and further intensify. Similar findings, although from a different perspective, are presented in Gray *et al*. (2024). Using reanalysis data, they produced a global climatology of intense warm-seclusion cyclones with and without sting jet precursors, showing that cyclones with the potential for sting jet descent (irrespective of its actual occurrence, which the data could not properly resolve) display more vigorous diabatic processes and are more likely to have crossed the upper-level jet during their intensification. Hence, considering the literature presented here, a link emerges between surface cyclones mainly driven by diabatic processes in their early development, subsequent upper-level jet crossing, rapid intensification and later evolution into warm-seclusion sting jet capable intense cyclones, consistent with our analysis of the evolution of Storm *Ciarán*.

It is also worth noting that the infamous Storm *Lothar*, which caused vast damage and loss of life over Central Europe (Wernli *et al*., 2002), is among the Shapiro–Keyser cyclones classified by Gray *et al*. (2024) as having sting jet precursors. This builds an interesting parallel with Storm *Ciarán*. *Lothar* initially developed as a DRW and, similarly to *Ciarán*, the subsequent jet crossing of the surface cyclone was associated

with a rapid 'bottom-up' intensification, in which cloud diabatic heating still played a primary role (Rivière *et al*., 2010; Čampa and Wernli, 2012). Even though those studies connected the extreme impacts of *Lothar* with its rapid propagation and intense low-level vorticity core, the case of Storm *Ciarán* suggests that descending sting jets might be an additional cause of impacts specifically related to the development of intense windstorms from rapidly deepening DRWs.

As this specific pathway of cyclone evolution from DRW to deep warm-seclusion, sting jet-bearing cyclone seems to be connected with the genesis of some of the most extreme windstorms hitting Europe, we believe it is key to explicitly highlight it and study it in a systematic way. Such an analysis would be timely, as the diabatic contribution to extratropical cyclones is expected to become more dominant in a warmer climate (Catto *et al*., 2019) and global ocean heat content is reaching record values (Copernicus, 2024). Interestingly, the potential relevance of anomalously high sea-surface temperature for the genesis of Storm *Lothar* was already discussed two decades ago by Wernli *et al*. (2002), as they highlighted in their final remarks the importance of low-level diabatic processes '*when discussing the possible implications of climate variability and change on the development of North Atlantic winter storms*'.

Acknowledgements

The authors would like to thank Maxi Boettcher (Kantonspolizei Zürich) and Michael Sprenger (ETH Zürich) for the support in running the DRW diagnostic tool. The work performed by Ambrogio Volonté was funded by the 2024 pump-priming fund of the Department of Meteorology, University of Reading. Jacopo Riboldi acknowledges funding from the Swiss National Science Foundation (SNSF) via grant PZ00P2_209135.

Author contributions

Ambrogio Volonté: Conceptualization; visualization; writing – original draft; writing – review and editing; formal analysis; methodology. **Jacopo Riboldi:** Conceptualization; visualization; writing – original draft; writing – review and editing; formal analysis; methodology.

Conflict of interest statement

The authors declare no competing interests.

Data availability statement

No new datasets were created in this study. ERA5 reanalysis data are publicly available at https://cds.climate.copernicus.eu/.

References

Binder H, **Boettcher M**, **Joos H** *et al*. 2016. The role of warm conveyor belts for the intensification of extratropical cyclones in northern hemisphere winter. *J. Atmos. Sci.* **73**: 3997–4020. https://doi.org/10.1175/JAS-D-15-0302.1

Bjerknes A. 1919. On the structure of moving cyclones. *Geofys. Publ.* **1**: 1–8.

Bjerknes A, **Solberg H**. 1922. Life cycle of cyclones and the polar front theory of atmospheric circulation. *Geofys. Publ.* **3**: 3–18.

Boettcher M, **Wernli H**. 2011. Life cycle study of a diabatic Rossby wave as a precursor to rapid cyclogenesis in the north Atlantic—dynamics and forecast performance. *Mon. Weather Rev.* **139**: 1861–1878. https://doi.org/10.1175/2011MWR3504.1

Boettcher M, **Wernli H**. 2013. A 10-yr climatology of diabatic Rossby waves in the northern hemisphere. *Mon. Weather Rev.* **141**: 1139–1154. https://doi.org/10.1175/MWR-D-12-00012.1

Browning KA. 2004. The sting at the end of the tail: damaging winds associated with extratropical cyclones. *Q. J. R. Meteorol. Soc.* **130**: 375–399.

Browning KA, **Field M**. 2004. Evidence from Meteosat imagery of the interaction of sting jets with the boundary layer. *Meteorol. Appl.* **135**: 663–680.

Čampa J, **Wernli H**. 2012. A PV perspective on the vertical structure of mature midlatitude cyclones in the northern hemisphere. *J. Atmos. Sci.* **69**: 725–740. https://doi.org/10.1175/JAS-D-11-050.1

Catto JL. 2016. Extratropical cyclone classification and its use in climate studies. *Rev. Geophys.* **54**: 486–520. https://doi.org/10.1002/2016RG000519

Catto JL, **Ackerley D**, **Booth JF** *et al*. 2019. The future of midlatitude cyclones. *Curr. Clim. Chang. Rep.* **5**: 407–420. https://doi.org/10.1007/s40641-019-00149-4

Clark PA, **Gray SL**. 2018. Sting jets in extratropical cyclones: a review. *Q. J. R. Meteorol. Soc.* **144**: 943–969. https://doi.org/10.1002/qj.3267

Copernicus: https://climate.copernicus.eu/climate-indicators/ocean-heat-content, 2024.

Cordeira JM, **Bosart LF**. 2011. Cyclone interactions and evolutions during the "perfect storms" of late october and early november 1991. *Mon. Weather Rev.* **139**: 1683–1707. https://doi.org/10.1175/2010MWR3537.1

Coronel B, **Ricard D**, **Rivière G** *et al*. 2015. Role of moist processes in the tracks of idealized midlatitude surface cyclones. *J. Atmos. Sci.* **72**: 2979–2996. https://doi.org/10.1175/JAS-D-14-0337.1

Coronel B, **Ricard D**, **Rivière G** *et al*. 2016. Cold-conveyor-belt jet, sting jet and slantwise circulations in idealized simulations of extratropical cyclones. *Q. J. R. Meteorol. Soc.* **142**: 1781–1796. https://doi.org/10.1002/qj.2775

Dacre H. 2020. A review of extratropical cyclones: observations and conceptual models over the past 100 years. *Weather* **75**: 4–7. https://doi.org/10.1002/wea.3653

Davies HC. 2015. The Quasigeostrophic Omega equation: reappraisal, refinements, and relevance. *Mon. Weather Rev.* **143**: 3–25. https://doi.org/10.1175/MWR-D-14-00098.1

Gray SL, **Volonté A**. 2024. Extreme Low-Level Wind Jets in Storm *Ciarán*. Weather. https://doi.org/10.1002/wea.7620

Gray SL, **Volonté A**, **Martínez-Alvarado O** *et al*. 2024. A global climatology of sting-jet extratropical cyclones, EGUsphere. Copernicus GmbH, pp 1–31. https://doi.org/10.5194/egusphere-2024-1413.

Hersbach H, **Bell B**, **Berrisford P** *et al*. 2020. The ERA5 global reanalysis. *Q. J. R. Meteorol. Soc.* **146**: 1999–2049. https://doi.org/10.1002/qj.3803

Hoskins BJ, **Draghici I**, **Davies HC**. 1978. A new look at the ω-equation. *Q. J. R. Meteor. Soc.* **104**: 31–38. https://doi.org/10.1002/qj.49710443903

Hoskins BJ, **McIntyre ME**, **Robertson AW**. 1985. On the use and significance of isentropic potential vorticity maps. *Q. J. R. Meteor. Soc.* **111**: 877–946. https://doi.org/10.1002/qj.49711147002

Moore RW, **Montgomery MT**. 2005. Analysis of an idealized, three-dimensional diabatic Rossby vortex: a coherent structure of the moist baroclinic atmosphere. *J. Atmos. Sci.* **62**: 2703–2725. https://doi.org/10.1175/JAS3472.1

Parker DJ, **Thorpe AJ**. 1995. Conditional convective heating in a baroclinic atmosphere: a model of convective frontogenesis. *J. Atmos. Sci.* **52**: 1699–1711. https://doi.org/10.1175/1520-0469(1995)052<1699:CCHIAB>2.0.CO;2

Raveh-Rubin S. 2017. Dry intrusions: Lagrangian climatology and dynamical impact on the planetary boundary layer. *J. Clim.* **30**: 6661–6682. https://doi.org/10.1175/JCLI-D-16-0782.1

Rivière G, **Laîné A**, **Lapeyre G** *et al*. 2010. Links between Rossby wave breaking and the North Atlantic Oscillation–Arctic Oscillation in present-day and Last Glacial Maximum climate simulations. *J. Clim.* **23**: 2987–3008. https://doi.org/10.1175/2010JCLI3372.1

Sanders F, **Gyakum JR**. 1980. Synoptic-dynamic climatology of the 'bomb'. *Mon. Weather Rev.* **108**: 1589–1606.

Schultz DM, **Keyser D**, **Bosart LF**. 1998. The effect of large-scale flow on low-level frontal structure and evolution in mid-latitude cyclones. *Mon. Weather Rev.* **126**: 1767–1791. https://doi.org/10.1175/1520-0493(1998)126<1767:TEOLSF>2.0.CO;2

Schultz DM, **Sienkiewicz JM**. 2013. Using frontogenesis to identify sting jets in extratropical cyclones in: weather and forecasting. *Weather Forecast.* **28**: 603–613. https://journals.ametsoc.org/view/journals/wefo/28/3/waf-d-12-00126_1.xml

Schultz DM, **Vaughan G**. 2011. Occluded fronts and the occlusion process: a fresh look at conventional wisdom. *Bull. Am. Meteorol. Soc.* **92**: 443–466.

Shapiro MA, **Keyser D**. 1990. Fronts, jet streams and the tropopause, in Extratropical Cyclones. Newton C, Holopainen EO (eds). American Meteorological Society & Springer, pp 167–191.

Stanković A, **Messori G**, **Pinto JG** *et al*. 2024. Large-scale perspective on extreme near-surface winds in the central North Atlantic. *Weather Clim. Dynam.* **5**: 821–837. https://doi.org/10.5194/wcd-5-821-2024

Thorncroft CD, **Hoskins BJ**, **McIntyre ME**. 1993. Two paradigms of baroclinic-wave life-cycle behaviour. *Q. J. R. Meteor. Soc.* **119**: 17–55. https://doi.org/10.1002/qj.49711950903

Wernli H, **Dirren S**, **Liniger MA** *et al*. 2002. Dynamical aspects of the life cycle of the winter storm 'Lothar' (24–26 December 1999). *Q. J. R, Meteor. Soc* **128**: 405–429. https://doi.org/10.1256/003590002321042036

Correspondence to: Ambrogio Volonté
a.volonte@reading.ac.uk

doi: 10.1002/wea.7632